Supporting Information

From coordination polymers to nanocrystals: General and facile synthesis of ultra-small metal oxide nanocrystals

Jiajia Zhang[†], Fang Cui*[, †], Li Li[‡], Yang Liu[†], and Tieyu Cui*[, †], Xiao Zhang[†]

[†]School of Chemistry and Chemical Engineering, Harbin Institute of Technology, Harbin 150001, China

[‡]State Key Laboratory of Inorganic Synthesis and Preparative Chemistry, College of Chemistry, Jilin University, Changchun 130012, China

E-mail: cuifang@hit.edu.cn，cuit@hit.edu.cn; Fax: (+86) 451-86403646; Tel: (+86)451-86403646;

EXPERIMENTAL

Chemicals

Methacrylic acid (MAA, 99.0%) and methyl methacrylate (MMA, 99.0%) were purchased from Aladdin Reagent Company (Shanghai, PR China). ZnO powder (99.0%), *N,N*-dimethylformamide (DMF, 99.0%) and absolute ethanol were purchased from Sinopharm Chemical Reagent Co., Ltd (Shanghai, PR China). The water used in the experiments was deionized with a resistivity of 18.2 MΩ $cm^{-1.}$ 2,2-Azobisisobutyronitrile (AIBN, 99.0%, Fisher) was recrystallized twice from ethanol. MAA and MMA were distilled before use. Other chemicals were used as received.

Synthesis of $Zn(MAA)_2$ nanoribbons

The synthesis of $Zn(MAA)_2$ nanoribbons is based on the literature we reported earlier[1]. Typically, ZnO powder (8.1 g, 0.1 mol) was reacted with MAA (17.2 g, 0.2 mol) in a round bottomed flask containing 150 mL deionized water under continuously stirred for at least 0.5 h at room temperature. After filtration, the clear $Zn(MAA)_2$ precursor aqueous solution of Zn^{2+} and MAA^- ions was prepared. Then 10 mL absolute ethanol was added into 10 mL $Zn(MAA)_2$ precursor aqueous solution, and the mixture was maintained at room temperature. Subsequently, the $Zn(MAA)_2$ nanoribbons were spontaneously formed in the water/ethanol mixture, and the nanoribbons were collected by centrifugation and washed with absolute ethanol.

Synthesis of ZnO QDs/$Zn(MAA)_2$ nanoribbons and ZnO quantum dots

In a typical procedure, the fresh $Zn(MAA)_2$ nanoribbons (undried, 6.0 g) were added into a solution of 10 mL deionized water, 10 mL absolute ethanol and 1 mL

DMF. After vigorous stirring for 10 min, the mixture was transferred into a Teflon-lined autoclave of 50 mL inner volume, sealed and heated at 100 °C for 7 h, then the reactor was allowed to cool down to room temperature naturally. After centrifugation of the mixture and washed with absolute ethanol, ZnO QDs/$Zn(MAA)_2$ nanoribbons were prepared. When the dosage of DMF is changed from 1 mL to 5 mL, there were no residual nanoribbons in the reactor, but the solution containing ZnO QDs was obtained. Then the solvent was removed with the aid of a rotary evaporator, and the residue was purified by dialysis to provide the desired product. Moreover, the solid samples of ZnO QDs can be obtained by freeze-drying. About 6.0 g of fresh (undried) $Zn(MAA)_2$ nanoribbons could be prepared only using 10 mL absolute ethanol and 10 mL $Zn(MAA)_2$ precursor aqueous solution, then around 20 mL ZnO QDs solution (50 mg after freeze-drying) could be synthesized using the above 6.0 g of fresh $Zn(MAA)_2$ nanoribbons. The experimental process is simple and easy to operate, which can be easily scaled up or done in parallel.

Synthesis of ZnO QDs/PMMA composite

The preparation of the ZnO QDs/PMMA composite was achieved via an in suit bulk polymerization method as follows: 2 mg ZnO QDs, 2 mL MMA and 3.93 mg AIBN were charged into a 10 mL weighing bottle, and the mixture was dispersed with ultrasonic vibration, bubbling with nitrogen (N_2). The subsequent bulk polymerization was carried out with the prepolymerization process at 60 °C for 15 min and the subsequent programmed heating process of 60 °C for 2 h, 70 °C for 2 h, 80 °C for 1 h, 90 °C for 1.5 h, 100 °C for 1.5 h and 120 °C for 1 h. And neat ZnO QDs/PMMA

composite was directly prepared after cooling to room temperature.

Synthesis of $Ca(MAA)_2$ nanoribbons

The synthesis of $Ca(MAA)_2$ nanoribbons is based on the literature we reported earlier[2]. $Ca(OH)_2$ powder (7.4 g, 0.1 mol) and MAA (17.2 g, 0.2 mol) were dissolved in 200 mL deionized water under continuously stirred for at least 0.5 h at room temperature. After filtration, the clear $Ca(MAA)_2 \cdot H_2O$ precursor solution of Ca^{2+} and MAA^- ions was formed. Then 200 mL absolute ethanol was added in 10 mL $Ca(MAA)_2 \cdot H_2O$ precursor solution, and the mixture was maintained at room temperature for 10 min. Subsequently, the $Ca(MAA)_2$ nanoribbons were spontaneously formed in the water/ethanol mixture, and the nanoribbons were collected by centrifugation and washed with absolute ethanol.

Single crystal X-ray diffraction

All data were collected on an Agilent Technology SuperNova Eos Dual system with a (Mo-Kα, λ = 0.7107 Å) micro focus source and focusing multilayer mirror optics. The data were collected at a temperature of 293 K and processed using CrysAlis^{Pro}. The structures were solved and refined using full matrix least-squares based on F^2 using the SHELXS-2014 and SHELXL-2014 programs. All non-hydrogen atoms were refined anisotropic ally and the hydrogen atoms of the organic ligands were localized in their calculated positions and refined using the riding model.

Characterization

To examine the surface morphologies of products, SEM analyses were obtained by employing a Merlin Compact scanning electron microscope with primary electron

energy of 3 kV. A FEI Tecnai G2 F30 transmission electron microscope, using an accelerating voltage of 300 kV, was employed to examine the internal morphologies of products. AFM images were recorded using a Bruker Dimension Icon. In addition, FTIR spectra were taken on a Perkin Elmer Spectrum 100 FT-IR spectrometer. ^{1}H NMR spectra were measured in D_2O using a Bruker AVANCE500 500 MHz NMR spectrometer. TGA measurements were performed using a Netzsch STA 449C thermogravimetric analyzer. XRD data were collected on a Rigaku D/Max-2500 X-ray diffractometer using a Cu target radiation source. Fluorescence spectroscopy was performed with a Perkin Elmer LS 55 Fluorescence Spectrometer. UV-vis spectra were recorded using SHIMADZU UV-2450 UV-vis Spectrophotometer and HITACHI UH4150 UV–vis/NIR Spectrophotometer equipped an integrating sphere. The UV-vis spectra shown in Fig. S11, S17 and S18 were run in transmission mode. The UV-vis spectra shown in Fig. S7 were run in reflectance mode, and the data of reflection has been converted to absorbance by the instrument automatically.

Formation mechanism of $Zn(MAA)_2$ nanoribbons

Typically, the $Zn(MAA)_2 \cdot H_2O$ precursor solution containing Zn^{2+} and MAA^- ions with a molar ratio of around 1:2 was prepared through the reaction of ZnO and MAA in water, which was thermodynamically stable since the formation of hydrogen-bond network between hydrophilic COO^- groups of MAA^- and H_2O molecules. Obviously, this strong solvation effect of MAA^- is adverse to the self-assembly of Zn^{2+} and MAA^- ions, and hence, ethanol (Kamlet–Taft H-bond acceptor parameter: $\beta_{ethanol} = 0.75$, H-bond donor parameter: $\alpha_{ethanol} = 0.83$, $\alpha_{water} = 1.17$)[3] was shortlisted

for the initiation solvent to appropriately weaken the solvent effect and simultaneously induce the self-assembly. After a certain amount of ethanol was added into $Zn(MAA)_2 \cdot H_2O$ precursor solution with a certain volume and the mixture was stored at room temperature for at least 6 h, a milky viscous gel formed (Fig. 2a, inset). The self-assembly of Zn^{2+} and MAA^- ions into nanoribbons can happen in the temperature range from 5 ℃ to 60 ℃. Undoubtedly, the initiation solvent plays an important role in the self-assembly process according to the desolvation mechanism. In addition to ethanol, isopropanol and diethylene glycol have been proved experimentally that can be as initiation solvents to prepare $Zn(MAA)_2$ nanoribbons (Fig. S3). Just like the coordination polymers we reported early, $Zn(MAA)_2$ nanoribbons also exhibit highly crystalline structures demonstrated by the powder X-ray diffraction (XRD) pattern (Fig. S4). The diffraction peaks in the XRD pattern appear at 9.94, 11.03, 11.95, 12.92, 13.41, 14.01, 16.72, 17.42, 17.91, 19.16, 19.42, 20.36, 21.05, 21.46, 22.16, 23.16, 24.11, 24.87, 25.97, 27.10, 27.79, 28.51, 29.28 and 30.18°, consistent with the (200), (101), (210), (111), (020), (201), (220), (121), (301), (311), (221), (102), (410), (112), (401), (131), (022), (302), (421), (331), (511), (430), (141) and (521) planes, respectively, of orthorhombic $Zn(MAA)_2$ (JCPDS no. 161140). In order to study the structure of $Zn(MAA)_2$ nanoribbons at a molecular level in detail, single crystal was successfully cultivated using $Zn(MAA)_2 \cdot H_2O$ precursor solution because of the similar desolvation formation mechanism. As expected, by comparing measured and simulated results, it could be found that the vast majority of peaks in XRD pattern of $Zn(MAA)_2$ nanoribbons are in good

agreement with the calculated XRD indexing result of single crystal (Fig. S4). Of course, we also note that the XRD pattern of $Zn(MAA)_2$ nanoribbons has several more peaks than that of the single crystal, which may be due to a slight change in the molecular arrangement of the nanoribbons during the centrifugal cleaning process. Thus, the detailed crystal structure of $Zn(MAA)_2$ nanoribbons can still be obtained by analyzing the single crystal. As shown in Table S1 and Fig. S5, is the Crystallographic data and X-ray crystal structure of $Zn(MAA)_2$, which has orthorhombic unit cells (space group Pna21) with lattice constants a = 1.783, b = 0.901, and c = 1.320 nm (Fig. S5b). The structure has been issued to CCDC and the CCDC number is 1865413. Moreover, the crystal exhibits a 1D structure along the c axis (Fig. S5a), which resembles the morphology of the $Zn(MAA)_2$ nanoribbons.

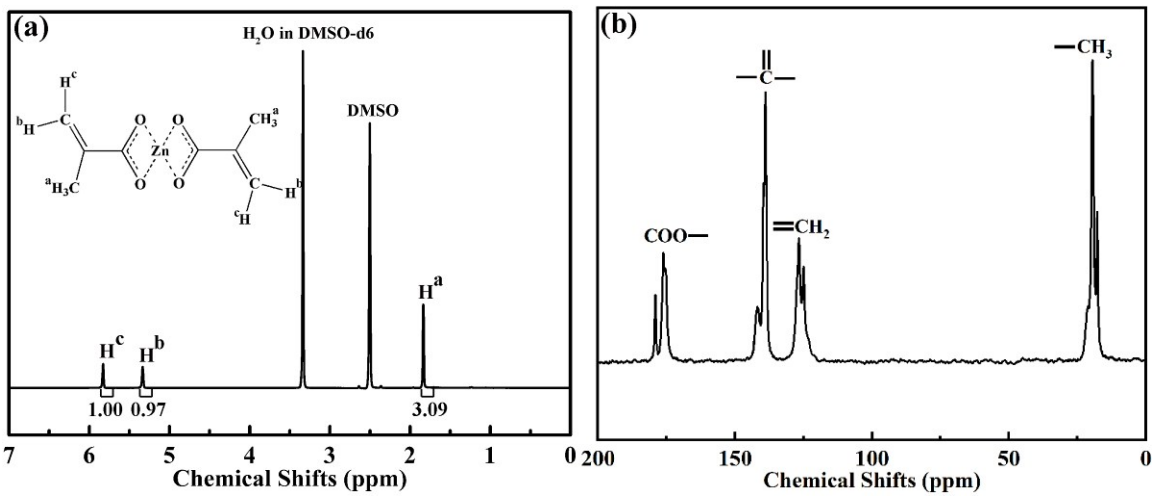

Fig. S1 ^{1}H NMR spectrum of $Zn(MAA)_2$ nanoribbons (a), ^{13}C ssNMR spectra of $Zn(MAA)_2$ nanoribbons (b).

Fig. S1 (a) shows the ^{1}H NMR spectrum and detailed peak assignments of $Zn(MAA)_2$ nanoribbons. The signals appearing at 1.835, 5.335 and 5.828 ppm, with an integral ration close to 3:1:1, can be assigned to the methyl (H^a) and two types of methylene (H^b and H^c) protons of the methacrylate ion (MAA^-). As presented in Fig.

S1 (b), the signals of ^{13}C ssNMR spectrum of nanoribbons appearing at 19.357, 126.768, 138.652 and 176.065 ppm can be well corresponded to various hybrid types of carbon of $Zn(MAA)_2$ structure.

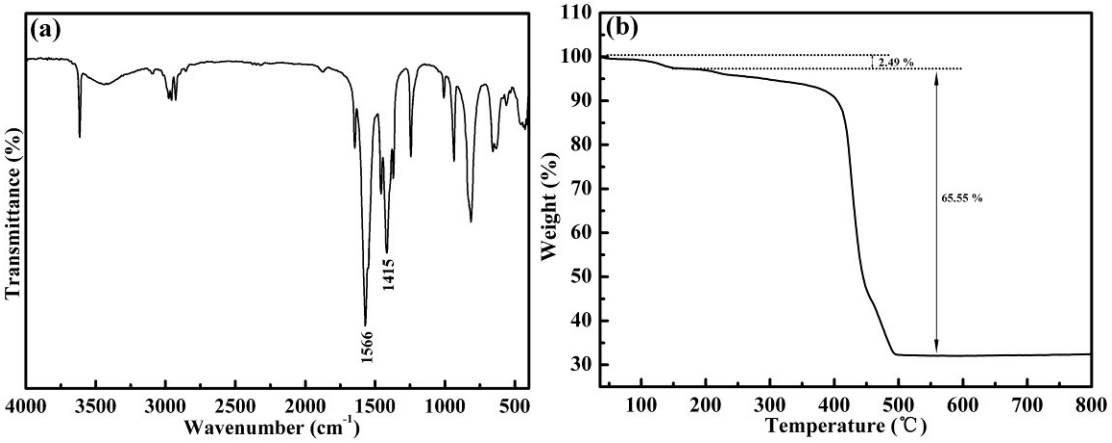

Fig. S2 FTIR spectrum (a) and TGA curve (b) of $Zn(MAA)_2$ nanoribbons.

The characteristic asymmetric and symmetric stretching vibrations peaks of carboxylate groups, appearing at around 1566 and 1415 cm^{-1} respectively in the FTIR spectrum (Fig. S2a) of the $Zn(MAA)_2$ nanoribbons, confirm the successful coordination of MAA^- and Zn^{2+} ions. TGA curve (obtained under O_2 atmosphere, heating rate: 10 ℃ min^{-1}) of $Zn(MAA)_2$ nanoribbons (Fig. S2b) further confirms the formula of $Zn(MAA)_2$. The weight loss of 2.49 % before 150 ℃ is assigned to the loss of crystal water. And the complete decomposition temperature is about 500 ℃, ZnO is obtained finally since the weight loss from 150 to 500 ℃ is about 65.55%, which is in agreement with the calculated value of 65.37%.

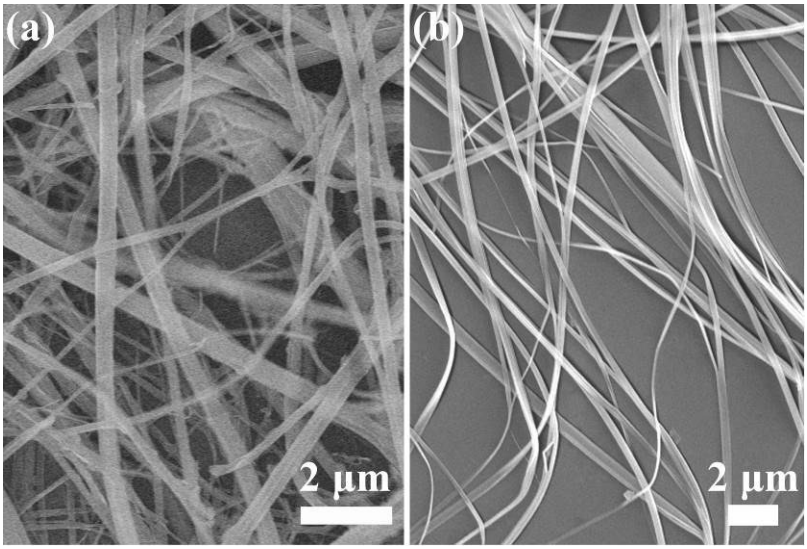

Fig. S3 SEM images of the $Zn(MAA)_2$ nanoribbons prepared by using isopropanol (a) and diethylene glycol (b) as the initiation solvents respectively.

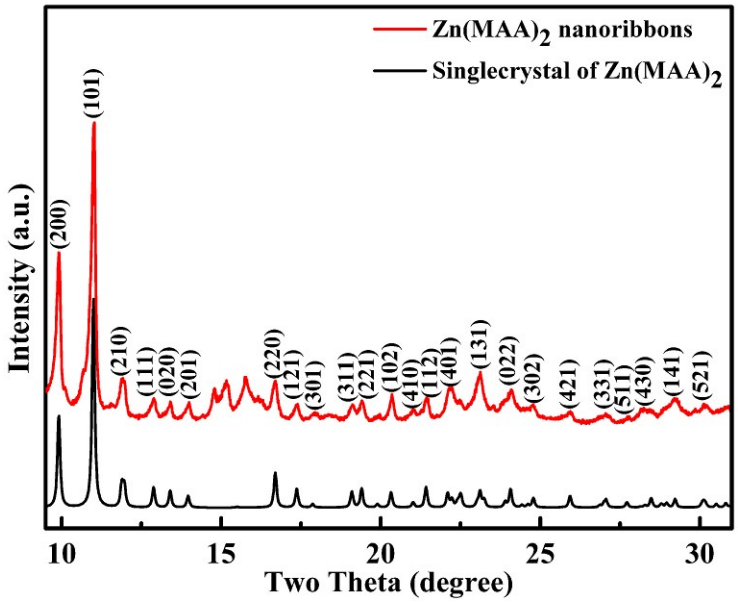

Fig. S4 XRD patterns of $Zn(MAA)_2$ nanoribbons and the single-crystal of $Zn(MAA)_2$.

Table S1 Crystallographic data of $Zn(MAA)_2$

Empirical formula	$C_{16}H_{20}O_8Zn_2$
Formula weight	471.06
Crystal system	Orthorhombic
Space group	Pna21
a/Å	17.8332
b/Å	9.0061

c/Å	13.2032
V/Å^3	2120.53 (9)
Z	4
Dc/Mg mm^{-3}	1.475
μ/mm^{-1}	2.297
F(000)	960.0
Radiation	MoKα (λ = 0.71073)
Reflections collected	5890
Independent reflections	6002 [R_{int}= 0.0245, R_{sigma}= 0.0310]
Data/restraints/parameters	2930/1/239
Goodness-of-fit on F^2	1.070
Final R indexes [I ≥ 2σ(I)]	R_1= 0.0299, wR_2= 0.0637
Final R indexes [all data]	R_1= 0.0360, wR_2= 0.0675

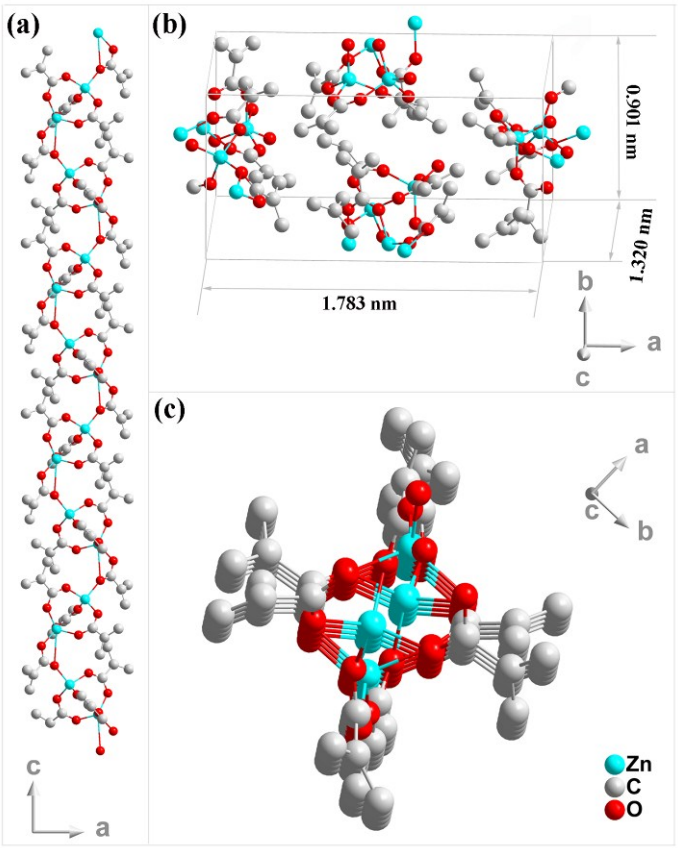

Fig. S5 X-ray crystal structure of Zn(MAA)$_2$.

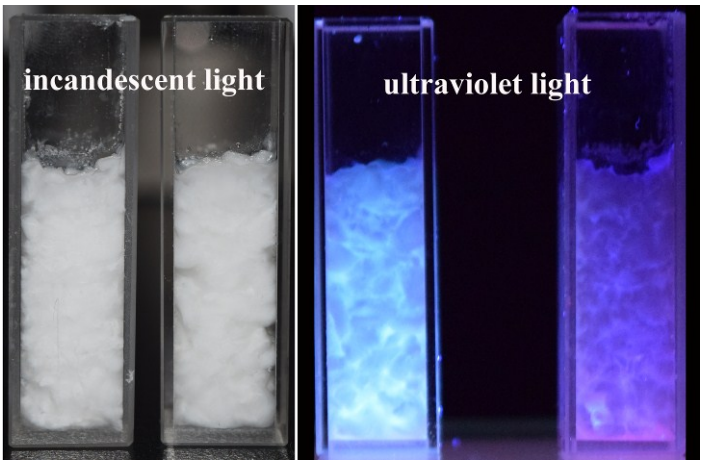

Fig. S6 Digital photos of ZnO QDs/$Zn(MAA)_2$ nanoribbons (left) and $Zn(MAA)_2$ nanoribbons (right) under incandescent light and ultraviolet light radiation (365 nm) respectively.

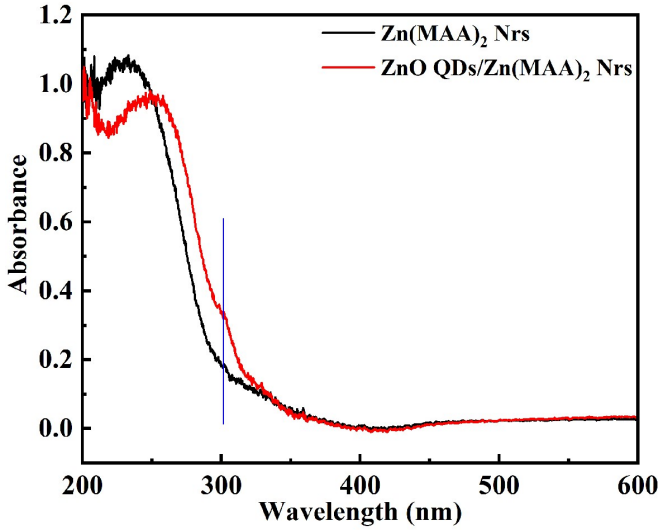

Fig. S7 UV-Vis absorption spectra of $Zn(MAA)_2$ and ZnO QDs/$Zn(MAA)_2$ nanoribbons.

Fig. S7 shows the UV-Vis absorption spectra of $Zn(MAA)_2$ and ZnO QDs/$Zn(MAA)_2$ nanoribbons. $Zn(MAA)_2$ nanoribbons display a absorption peak at around 230 nm, owing to the possible formation of conjugated double bonds during the self-assembly of nanoribbons. Compared with that of $Zn(MAA)_2$ nanoribbons, the absorption peak of ZnO QDs/$Zn(MAA)_2$ nanoribbons appear red-shifted (centered at 250 nm) and a new absorption peak appears at 300 nm. The new peak at 300 nm is due to the formation of ZnO QDs, and the red-shift may be due to the change in the structure of the nanoribbons and the reduction of the number of conjugated double bonds during the formation of the ZnO QDs.

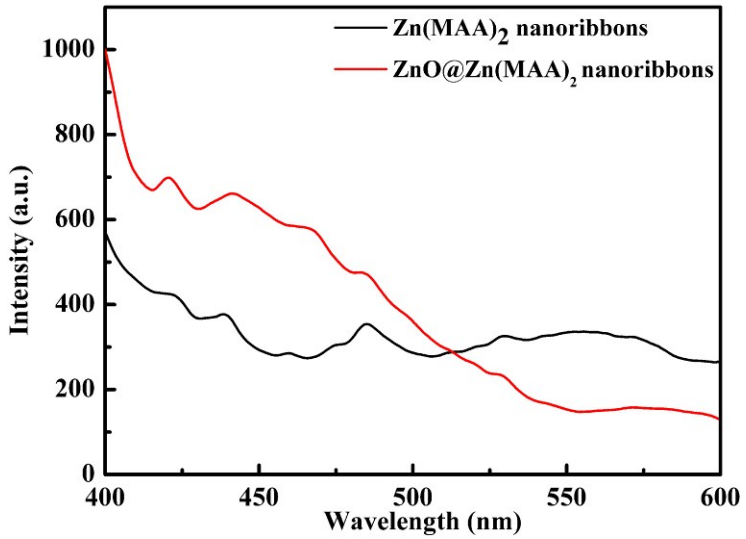

Fig. S8 Fluorescence spectra of $Zn(MAA)_2$ and ZnO QDs/$Zn(MAA)_2$ nanoribbons (The samples were excited by 365 nm light to record the PL emission).

In order to investigate the mechanism of nanoribbon destruction with increasing levels of DMF, some control experiments are carried out. Under high temperature and pressure conditions, DMF is partially hydrolyzed into formic acid and dimethylamine. Dimethylamine can provide an alkaline environment for the formation of ZnO QDs, while formic acid provides protons for the destruction of $Zn(MAA)_2$ nanoribbons. Experiment shows that only 400 μL of formic acid is needed to destruct $Zn(MAA)_2$ nanoribbons prepared using 10 mL absolute ethanol and 10 mL precursor solution at room temperature, shown in Fig. S9c. Moreover, $Zn(MAA)_2$ nanoribbons can also be partially decomposed in hydrothermal treatment under alkaline conditions, diethylamine was selected as an example and the result is shown in Fig. S9d. Comparing the photos of nanoribbons before and after hydrothermal treatment with diethylamine, it can be seen that most of the nanoribbons were destroyed while the solution obtained is yellow, which may be caused by the defects and aggregation of obtained ZnO nanoparticles. In addition, other solvents are also selected for control

experiments and the results are shown in Fig. S9 and Table S2. It can be concluded that only solvents with a structure similar to DMF can destroy $Zn(MAA)_2$ nanoribbons and release the QDs. The nanoribbon destruction is mainly dependent on the decomposition of DMF and is also associated with pH.

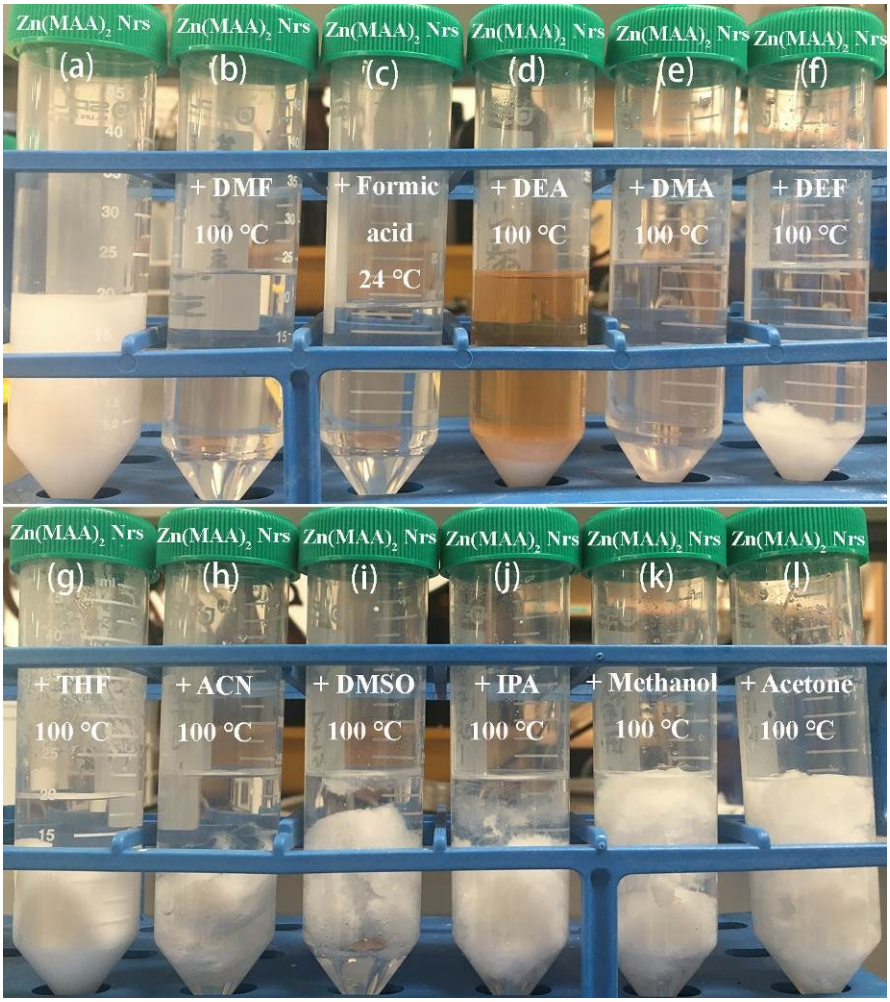

Fig. S9 Digital photos of the state of $Zn(MAA)_2$ nanoribbons under different solvent conditions.

Table S2 Results of destruction of $Zn(MAA)_2$ nanoribbon after hydrothermal treatment with the same condition.

solvents	nanoribbon destruction
N, N-Dimethylformamide (DMF)	totally
Diethylamine (DEA)	mostly
N, N-Dimethylacetamide (DMA)	mostly

N, N-Diethylformamide (DEF)	partially
Tetrahydrofuran (THF)	little
Acetonitrile (ACN)	little
Dimethyl sulfoxide (DMSO)	no
Isopropanol (IPA)	no
Methanol	no
Acetone	no

The stability of as-prepared ZnO QDs released from the nanoribbons is quite good and there is no aggregation of QDs during five months of storage, which can be testified by the original digital photos taken at different time of the same batch of ZnO QDs solution under 365 nm ultraviolet light radiations, shown in Fig. S10.

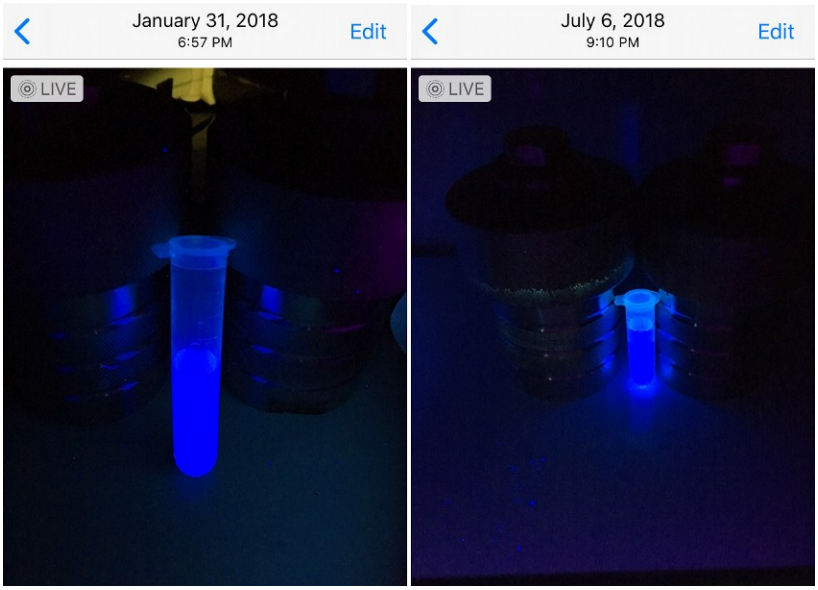

Fig. S10 The original digital photos taken at different time of the same batch of ZnO QDs under 365 nm ultraviolet light radiation.

As shown in the Fig. S11, the UV-vis absorption spectrum of ZnO QDs aqueous solution displays an absorption peak at around 265 nm and the absorption onset is about 300 nm. It can be concluded from the Fig. S11 that the corresponding size of ZnO QDs existed in solution is less than 2.5 nm according to the plots of absorption onset and band gap enlargement versus particle diameter for ZnO obtained from the effective mass model (Brus model) reported in literature[4], which is consistent with the result of HRTEM.

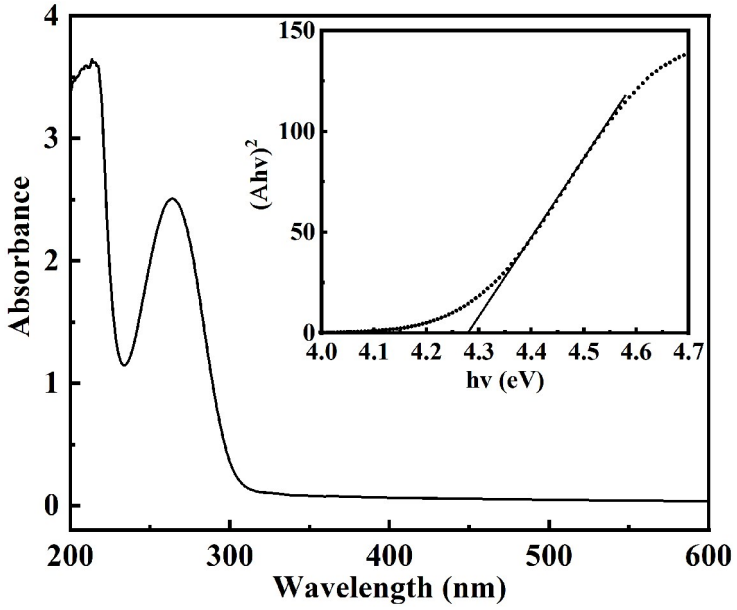

Fig. S11 UV-vis absorption spectrum of ZnO QDs aqueous solution, and the inset is the corresponding Tauc plot of $(Ahv)^2$ versus hv for the evaluation of the band gap ($E^* = 4.28$ eV).

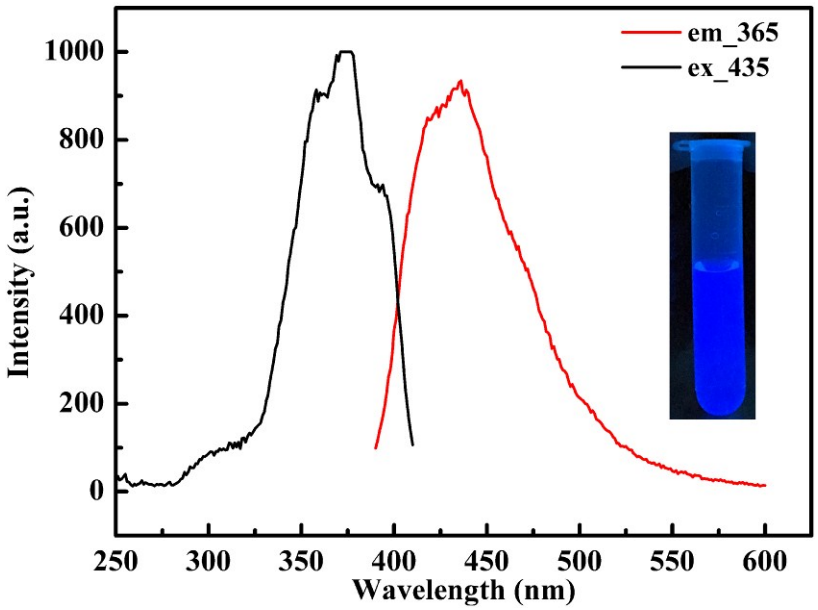

Fig. S12 Fluorescence spectra of ZnO QDs aqueous dispersion (The sample was excited by 365 nm light to record the PL emission, while the excitation spectrum was obtained by setting 435nm as the emission maximum). The inset is a digital photo of ZnO QDs under 365 nm ultraviolet light radiation.

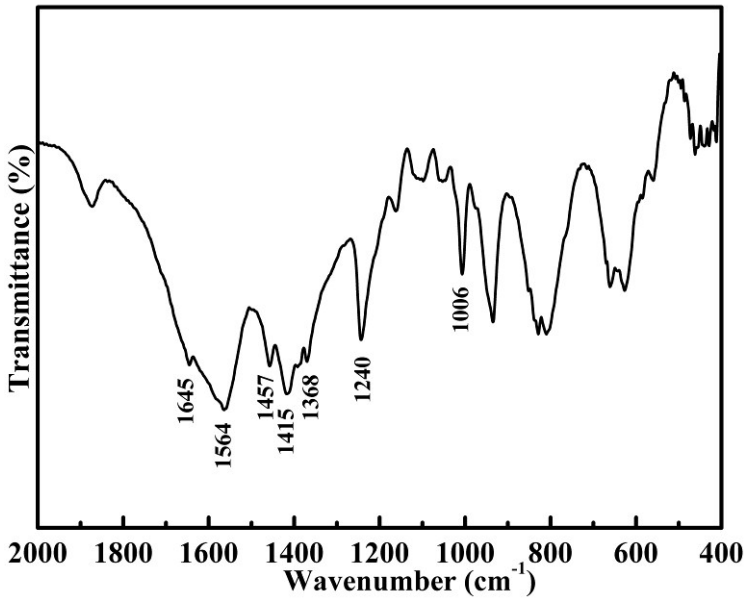

Fig. S13 FTIR spectrum of ZnO QDs.

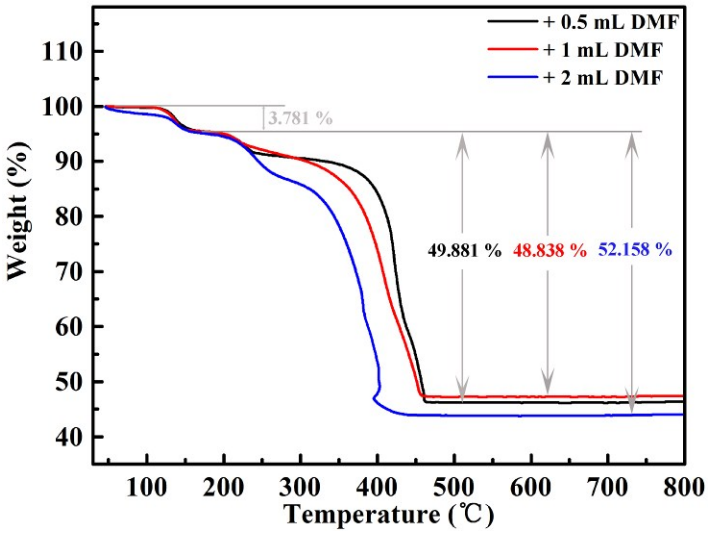

Fig. S14 TGA curves of ZnO QDs/$Zn(MAA)_2$ nanoribbons prepared through using different dosages of DMF.

The mass loss of pure $Zn(MAA)_2$ nanoribbons from 150 to 500 ℃ is about 65.55% (Fig. S2). However, after the nanoribbons were treated with 0.5 mL DMF, the mass loss is reduced to 49.881%, indicating that the content of ZnO QDs increases and the structure of $Zn(MAA)_2$ nanoribbons is almost unchanged in this process. When the dosage of DMF is increased to 1 mL, the mass loss continues to decrease to 48.838%, showing the content of ZnO QDs is still increasing. Whereas, the mass loss of the nanoribbons instead increased to 52.158% when the dosage of DMF continues to increase to 2 mL, indicating that the structure of nanoribbons is damaged little by little in this process and the ZnO QDs are released into solution.

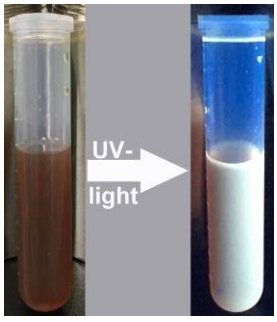

Fig. S15 Digital photos of ZnO QDs turbid liquid prepared using commercial $Zn(MAA)_2$ powder as precursor under incandescent light and ultraviolet light radiation (365 nm) respectively.

For comparison, we prepared ZnO QDs using commercial $Zn(MAA)_2$ powder as template in the same way. As shown in Fig. S11, the obtained ZnO QDs solution is brown turbid liquid, indicating the ZnO QDs could not be released completely when

the precursor is changed into commercial $Zn(MAA)_2$ powder. And the yellow-white fluorescence indicates that the particle size of ZnO QDs is larger according to the quantum size effect.

The $Zn(MAA)_2$ nanoribbons we prepared are formed by self-assembly based on desolvation, and the process is relatively mild and slow. As shown in Fig. S5, five Zn^{2+} and six MAA^- ions form a stable molecular cage with hydrophilic centers and hydrophobic surfaces through coordination firstly. And then in order to satisfy the four coordination of Zn^{2+}, these molecular cages are bridged by other MAA^- ions along the c axis of the unit cell to form 1D molecular chain. Finally molecular chains are packed orderly into nanoribbons by the inter-chain van der Waals force. Therefore, when ZnO QDs are formed in situ, ultra-small size can be guaranteed since Zn^{2+} ions are well arrangement in the longer 1D molecular chain, which plays a good role in confinement to prevent aggregation of ZnO QDs in the same or different molecular chains. It can be seen that the formation process of nanoribbons is carried out in stages, so the process of nanoribbons being destroyed to release ZnO QDs is also carried out in reverse. The inter-chain van der Waals forces between molecular chains are easy and firstly broken, and the longer molecular chains containing ZnO QDs are further destroyed into several shorter chain fragments to release ZnO QDs. In general, the phased process is easier. Therefore, the nanoribbon geometry is necessary to obtain small ZnO nanoparticles.

However, the commercial $Zn(MAA)_2$ is a nanocrystal with a size of several tens of nanometers obtained by chemical precipitation. The chemical precipitation is faster, thus the nucleation and growth rate of commercial $Zn(MAA)_2$ crystal is faster. And in a short time, Zn^{2+} and MAA^- ions tend to form more coordination to be stabilized. At the same time, there is no proper solvent environment to align the hydrophilic and hydrophobic groups of MAA^- ions. First of all, ZnO QDs may agglomerate during the formation process, because there is no confined effect of a longer molecular chain and there is a possibility of collision since the distribution of Zn^{2+} ions is messy. Then, there is less intermolecular force existed in the crystal structure of commercial $Zn(MAA)_2$ and the entire crystal network structure should be destroyed at one time to

release ZnO QDs, which is relatively difficult. Thus, commercial $Zn(MAA)_2$ does not provide nanoparticles with the same quality and cannot be fully released.

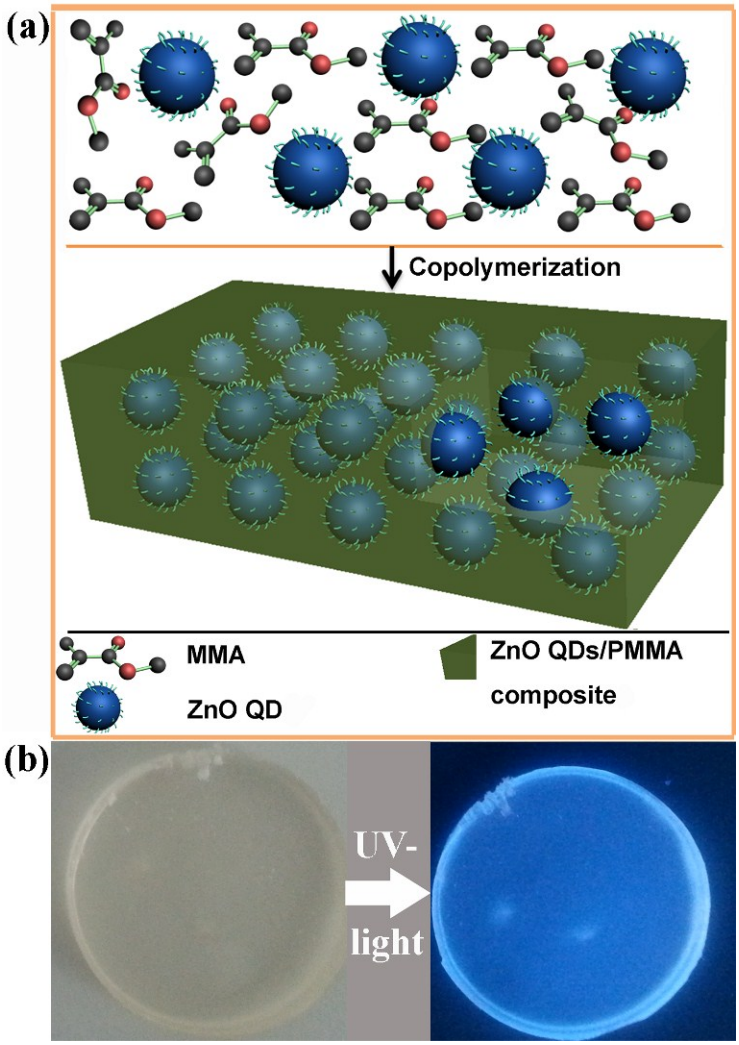

Fig. S16 (a) The synthetic pathway for the preparation of ZnO QDs/PMMA composite. (b) Digital photos of ZnO QDs/PMMA composite under incandescent light and ultraviolet light radiation respectively.

In order to investigate the relationship between ZnO QDs loading and optical properties of ZnO QDs/PMMA composites, UV-vis absorbance and transimission spectra of ZnO QDs/PMMA composites with different loading levels of ZnO QDs were characterized, as shown in Fig. S17. It can be concluded that the more ZnO QDs loading in PMMA, the more UV light is absorbed, while the smaller the light transmittance of the composites.

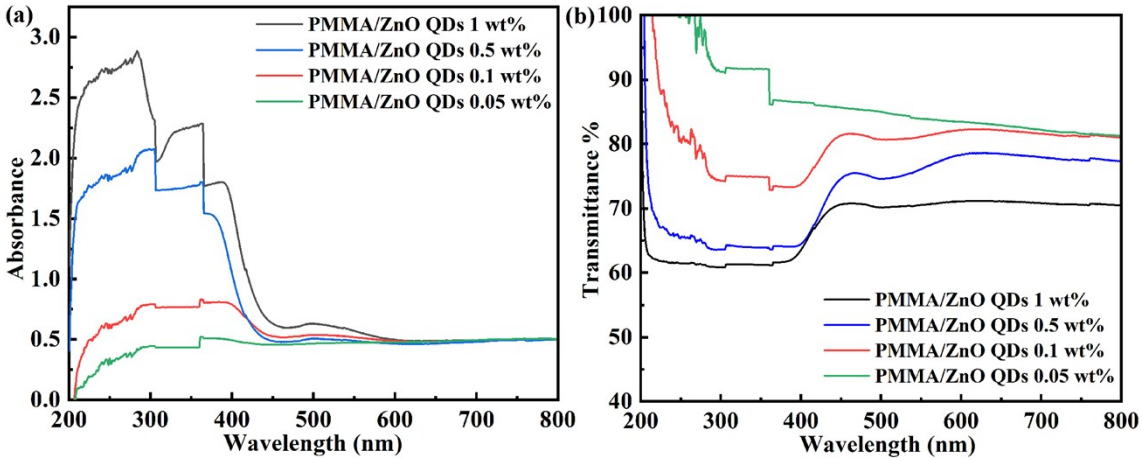

Fig. S17 UV-vis absorbance (a) and transimission (b) spectra of ZnO QDs/PMMA composites with different loading levels of ZnO QDs.

The UV-vis absorbance spectra of ZnO QDs/PMMA composites treated under different conditions, shown in Fig. S18. It can be seen that the UV-vis absorbance spectrum of ZnO QDs/PMMA composite has almost no change after irradiation with UV lamp (365 nm) for 48 h and has a little decrease after soaking in 80 ℃ water for 48 h. Therefore, the as-prepared ZnO QDs/PMMA composite is relatively stable and may be used in optical field under different conditions.

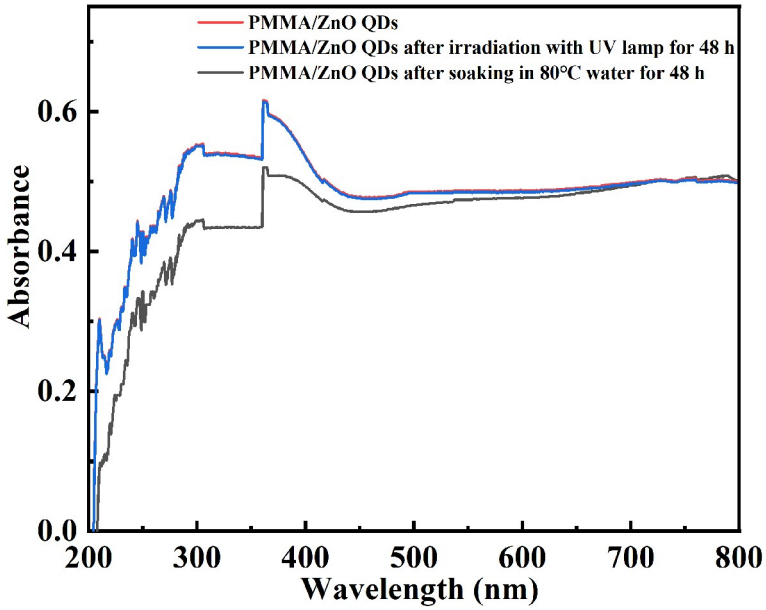

Fig. S18 UV-vis absorbance spectra of ZnO QDs/PMMA composites treated under different conditions.

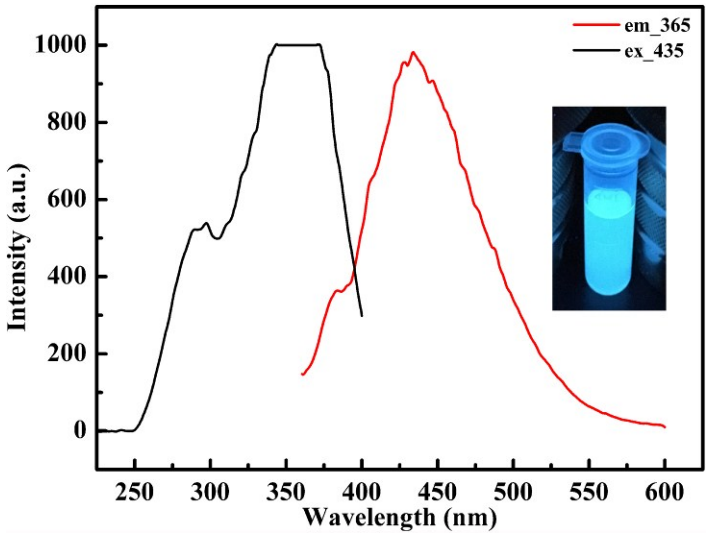

Fig. S19 Fluorescence spectra of CaO nanocrystals aqueous dispersion (The sample was excited by 365 nm light to record the PL emission, while the excitation spectrum was obtained by setting 435nm as the emission maximum). The inset is a digital photo of CaO nanocrystals under 365 nm ultraviolet light radiation.

Reference

1. Liu, M.; Cui, F.; Ma, Q.; Xu, L.; Zhang, J.; Zhang, R.; Cui, T., Janus coordination polymer derived PdO/ZnO nanoribbons for efficient 4-nitrophenol reduction. *New Journal of Chemistry* **2020**.

2. Zhang, J.; Cui, F.; Xu, L.; Pan, X.; Wang, X.; Zhang, X.; Cui, T., The development of novel Au/CaO nanoribbons from bifunctional building block for biodiesel production. *Nanoscale* **2017,** *9* (41), 15990-15997.

3. Kamlet, M. J.; Taft, R., The solvatochromic comparison method. I. The. beta.-scale of solvent hydrogen-bond acceptor (HBA) basicities. *Journal of the American chemical Society* **1976,** *98* (2), 377-383.

4. Pesika, N. S.; Stebe, K. J.; Searson, P. C., Determination of the Particle Size Distribution of Quantum Nanocrystals from Absorbance Spectra. *Advanced Materials* **2003,** *15* (15), 1289-1291.